Article

Effect of Lithium Salt Concentration on Materials Characteristics and Electrochemical Performance of Hybrid Inorganic/Polymer Solid Electrolyte for Solid-State Lithium-Ion Batteries

Debabrata Mohanty [1] ![ORCID], **Shu-Yu Chen** [1] **and I-Ming Hung** [1,2,]* ![ORCID]

[1] Department of Chemical Engineering and Materials Science, Yuan Ze University, Chung-Li 32003, Taiwan
[2] Hierarchical Green-Energy Materials (Hi-GEM) Research Center, National Cheng Kung University, Tainan 70101, Taiwan
[*] Correspondence: imhung@saturn.yzu.edu.tw; Tel.: +886-3-463-8800

Abstract: Lithium-ion batteries are popular energy storage devices due to their high energy density. Solid electrolytes appear to be a potential replacement for flammable liquid electrolytes in lithium batteries. This inorganic/hybrid solid electrolyte is a composite of lithium bis(trifluoromethanesulfonyl)imide (LiTFSI) salt, (poly(vinylidene fluoride-hexafluoro propylene) (PVDF-HFP) polymer and sodium superionic conductor (NASICON)-type $Li_{1+x}Al_xTi_{2-x}(PO_4)_3$ (LATP) ceramic powder. The structure, morphology, mechanical behavior, and electrochemical performance of this composite solid electrolyte, based on various amounts of LiTFSI, were investigated. The lithium-ion transfer and conductivity increased as the LiTFSI lithium salt concentration increased. However, the mechanical strength apparently decreased once the percentage of LITFSI was over 60%. The hybrid electrolyte with 60% LiTFSI content showed high ionic conductivity of 2.14×10^{-4} S cm^{-1}, a wide electrochemical stability window (3–6 V) and good electrochemical stability. The capacity of the Li | 60% LiTFSI/PVDF-HFP/LATP | LiFePO$_4$ solid-state lithium-metal battery was 103.8 mA h g^{-1} at 0.1 C, with a high-capacity retention of 98% after 50 cycles.

Keywords: solid-state battery; LiTFSI content; PVDF-HFP; hybrid electrolyte; lithium-ion mobility

1. Introduction

Electronic devices have become an indispensable element of human existence in recent years, due to fast advances in science and technology, Consequent to these advances, massive amounts of electricity are demanded. The need for energy is steadily growing. However, the world's fossil fuels are slowly depleting. Environmental consciousness is progressively growing globally, and alternative energy sources are being aggressively sought, thus, renewable energy is expected and is receiving a lot of attention. However, the search is now constrained by renewable energy's limits and the fact that the technology is not sophisticated enough to enable reliable applications. Electrochemical energy storage technology has progressed further and is more mature than many other energy storage technologies [1]. Lithium-ion batteries have been actively developed, due to the benefits of high energy and power density [2,3]. In comparison to other secondary batteries, secondary lithium-ion batteries have a reversible internal electrochemical reaction, which not only offers better electric capacity but also ensures long-term growth [4,5].

For a lithium-ion battery to perform well it should have the following characteristics: (1) high energy density, (2) high working voltage, (3) stable charging and discharging platform, (4) wide temperature range for use, (5) long storage life and good cycling, (6) no memory, (7) excellent safety, and (7) be light weight, amongst other benefits [6–11]. The research and demand for lithium-ion batteries are rising in tandem with the increase in environmental consciousness and the advent of hybrid electric vehicles (HEVs) and

electric cars (EVs) [12–14]. The electrochemical performance and safety of batteries has been improved by modifications and developments in electrolyte and electrode materials [15–18].

Organic liquid electrolytes with low ionic resistance are commonly used in lithium-ion batteries to aid the transport of lithium-ions between the positive and negative electrodes [19]. The electrolyte may leak if the battery case is damaged. Furthermore, lithium dendrites are easily formed on the surfaces of the two poles during the continuous charge and discharge operation, especially using lithium metal as the anode [20]. The battery might short-circuit or even explode if the lithium dendrites breach the separation membrane and contact the positive electrode. Solid-state batteries have many advantages, such as higher safety, being less hazardous, using electrolytes that are less flammable and having greater storage capacity [21,22], compared to batteries using liquid electrolytes. However, many forms of solid electrolytes are now experiencing issues that must be addressed, including a high interface resistance between cathode and anode electrodes, the need for improved ionic conductivity, widening of voltage range, demand for acceptable mechanical characteristics and high thermal stability [23,24]. The polymer solid electrolyte has the advantages of being soft and easy to process and it can adhere to the positive and negative electrodes well to alleviate the problem of high interface resistance [25]. However, the polymer electrolyte has to improve its ionic conductivity and solve the issue of instability in high-potential conditions because of the weak bonding of polymer molecules [26]. The use of a single material electrolyte has limits in terms of limiting the operating voltage and lowering the energy density. In recent years, there has been an increase in the number of studies combining polymers with inorganic materials [27,28]. Poly(vinylidene fluoride-hexafluoro propylene (PVDF-HFP) is a polymer electrolyte with a high dielectric constant and partially amorphous and partly crystalline structure. Ion conduction is improved as the amorphous phase of the polymer increases [29]. Polymer based on the crystalline phase has high mechanical properties. Furthermore, PVDF-HFP has a greater melting point (141–145 °C) than PEO-based electrolytes, which allows it to work at higher temperature environments [30,31]. $Li_{1+x}Al_xTi_{2-x}(PO_4)_3$ (LATP) has become a potential inorganic solid electrolyte due to its NASICON structure, which has good chemical and thermal stability and high ionic conductivity. However, when reduction of Ti^{4+} to Ti^{3+} in LATP occurs as it makes contact with lithium metal, the result is low ionic conductivity and high electronic conductivity [32–34].

In order to reduce the interface resistance and increase the ionic conductivity of solid electrolytes, the PVDF-HFP-LATP hybrid solid electrolyte was used as the main material. The effect of various contents of LiTFSI on the thermal stability, mechanical properties, ionic conductivity and electrochemical properties of the electrolyte membranes were investigated. A charge–discharge of $LiFePO_4$/solid electrolyte/Li metal cell, based on the optimal hybrid solid electrolyte membrane, was tested to show its potential for solid-state batteries.

2. Results and Discussion

The crystalline structures of LATP and hybrid electrolytes were investigated by X-ray diffraction (XRD) and the results are shown in Figure 1. Figure 1a shows that the diffraction peaks of LATP prepared by the sol-gel method, consisted of the NASICON structure of $LiTi_2(PO_4)_3$ (JCPDS 35-0754). Figure 1b shows that the diffraction peaks of PVDF-HFP were located at 18.99°, 20.57°, and 26.9°. Figure 1c–f shows the XRD patterns of hybrid electrolytes with different amounts of LiTFSI. In comparison to the XRD patterns of the LATP (Figure 1a) and hybrid electrolytes (Figure 1c–f), there was no significant difference in position of diffraction peaks for LATP, which meant the structure of LATP did not change during the preparation process of the PVDF-HFP-LATP-LiTFSI hybrid electrolytes. In addition, it was found that the diffraction peak intensity of PVDF-HFP steadily decreased and broadened with increasing amounts of LiTFSI and this meant the crystallization of PVDF-HFP polymer decreased. The diffraction peak of PVDF-HFP almost disappeared as the content of LiTFSI reached 70%. The phenomenon could be explained by the fact that ceramic LATP particles and the lithium salt of LiTFSI disrupted the bonding of the polymer

chain, resulting in the structure of PVDF-HFP polymer transferring from crystalline to amorphous. The result of previous studies [35] had shown that an improvement in the amorphous region of the polymer could increase lithium-ion mobility and conductivity. Therefore, it was expected that the lithium-ion conductivity of PVDF-HFP-LATP-LiTFSI hybrid electrolytes would increase with the increasing amount of LiTFSI. However, it was found that the physical state of the hybrid electrolyte contained as much as 70% LiTFSI as a gel, which was difficult to dry and form into a solid membrane. Therefore, it is recommended that the content of LiTFSI in PVDF-HFP-LiTFSI hybrid electrolytes should not be higher than 60%.
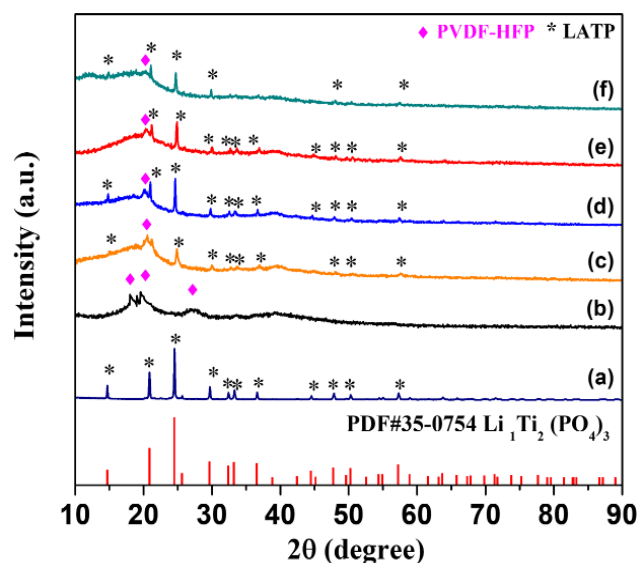

Figure 1. XRD patterns of (**a**) LATP, (**b**) PVDH-HFP, and hybrid electrolytes with different LiTFSI contents of (**c**) 40%, (**d**) 50%, (**e**) 60%, and (**f**) 70%.

The surface morphologies of the electrolyte membrane with varied LiTFSI contents were observed by FE-SEM, which are shown in Figure 2. There were a few white particles dispersed on the surface of the membranes. The average particle size of LATP powder synthesized by the citric acid-gel method was about 300 nm and the content of LATP in this hybrid electrolyte was 5%. Therefore, the LATP ceramic particles were uniformly dispersed and no serious agglomeration phenomena were observed. The surface of the hybrid membranes contained 50% and 60% LiTFSI lithium salt, shown in Figure 2b,c, and was partly uneven with rough morphology, compared to the sample containing 40% LiTFSI. This hybrid electrolyte membrane, prepared by the doctor blade method [36], was prepared on a polymer substrate and dried in the vacuum oven at 60 °C to evaporate the solvent. Irregular holes appeared on the surface of the electrolyte membrane due to the lower viscosity of slurry, as the LiTFSI lithium salt was higher than 50%. Several fractures occurred in the electrolyte membrane as the LiTFSI lithium salt concentration approached 70%, as illustrated in Figure 2d. The high content of LiTFSI weakened the link between polymer molecules, resulting in fractures after being strained during the drying process, due to the low mechanical strength of PVDF-HFP polymer electrolyte. However, the irregular holes did not penetrate the entire electrolyte membrane, so there was no risk of short circuit in the battery.
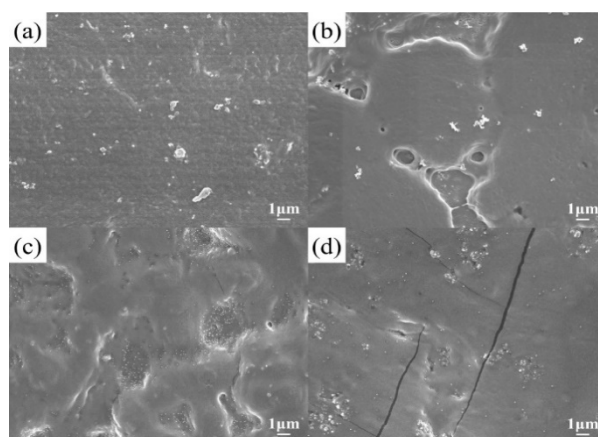
Figure 2. FE- SEM micrographs of electrolyte membranes with various LiTFSI contents of (**a**) LiTFSI-40%, (**b**) LiTFSI-50%, (**c**) LiTFSI-60%, and (**d**) LiTFSI-70%.

According to the results of the XRD, the crystallinity of the PVDF-HFP polymer decreased as the LiTFSI lithium salt increased. The DSC was employed to investigate the crystallization behavior of the hybrid electrolytes. An empty aluminum ingot and the samples were heated and cooled with 5 °C/min. The material's fundamental thermal characteristics, such as melting point (T_m), enthalpy change (ΔH), and crystallization temperature (T_c), were determined. Figure 3 shows the DSC spectra of electrolyte membranes with various LiTFSI contents. The kinetic energy of the molecules increased as the temperature rose, causing the structure of the polymer to change from crystalline to amorphous. An endothermic peak appeared as the polymer transformed from crystalline to molten and was determined as the endothermic peak's starting point, which was the melting point of the polymer (T_m). The T_m of the LiTFSI-40%, LiTFSI-50%, LiTFSI-60%, and LiTFSI-70% was 123.2 °C, 110.2 °C, 108.1 °C, and 110.5 °C, respectively.
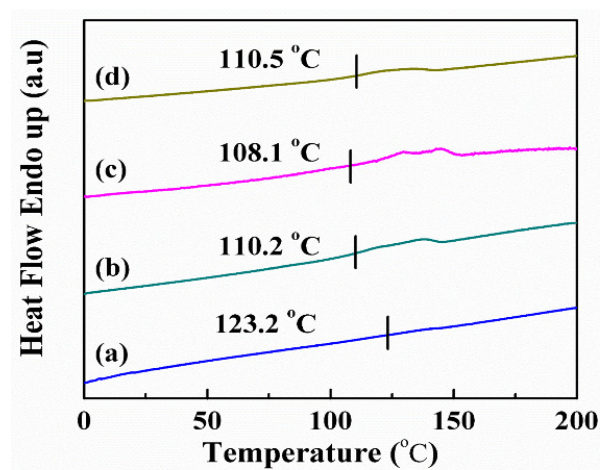

Figure 3. DSC spectra of electrolyte membranes with various LiTFSI content for (**a**) LiTFSI-40%, (**b**) LiTFSI-50%, (**c**) LiTFSI-60%, and (**d**) LiTFSI-70%.

One of material characteristic requirements for solid electrolytes is acceptable mechanical strength to prevent puncture by the lithium metal dendrite. The mechanical properties of the hybrid electrolyte membranes as indicated by a tensile machine are shown in Figure 4 and Table 1. The tensile strength of the hybrid electrolyte membrane decreased as the content of LiTFSI lithium salt increased. The tensile strength values of the LiTFSI-40%, LiTFSI-50%, LiTFSI-60%, and LiTFSI-70% were 4.42 MPa, 3.34 MPa, 2.06 MPa, and 0.32 MPa, respectively. The membrane with 40–60% LiTFSI showed high tensile strength and exhibited good, stable mechanical structure, leading to high safety of ASSLIB to pre-

vent short circuits during the charge/discharge process. The elongation values of the LiTFSI-40%, LiTFSI-50%, LiTFSI-60%, and LiTFSI-70% were 394.8%, 293.1%, 263.4%, and 60.89%, respectively. The hybrid electrolytes with 40–60% LiTFSI exhibited above 200% elongation to show high flexibility and good toughness. The mechanical properties of this hybrid electrolyte were mostly provided by the PVDF-HFP polymer. The link of polymer molecules was too weak as the LiTFSI content reached 70%, which was difficult to produce as a solid electrolyte.
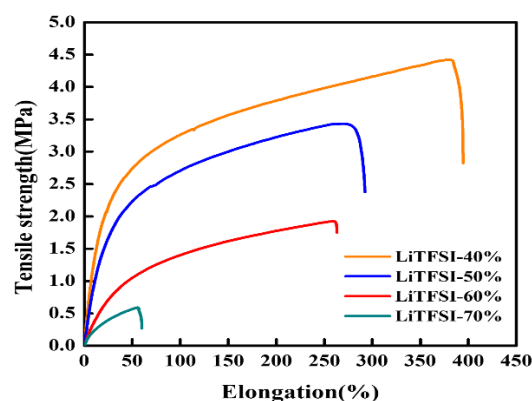

Figure 4. Mechanical properties of hybrid electrolyte with different contents of LiTFSI.

Table 1. Mechanical properties of hybrid electrolytes with various contents of LiTFSI.

Sample	Tensile Strength (MPa)	Elongation (%)
LiTFSI-40%	4.42	394.8
LiTFSI-50%	3.34	293.1
LiTFSI-60%	2.06	263.4
LiTFSI-70%	0.32	60.89

Recently, cathode materials have been developing higher potential and higher energy density. In order to achieve a more stable and safer lithium-ion battery, the electrolyte must be able to withstand high potential without structure decomposition. The electrochemical window of the electrolyte is determined by the linear sweep voltammetry (LSV) in the potential range of 2.5–6.0 V. Figure 5 shows the LSV of the electrolyte membranes with various LiTFSI contents. There was no apparent anodic current detected for the electrolyte membrane with LiTFSI lithium salt content increasing from 50–70% in the range of 2.5–4.7 V, which was lower to that of LiTFSI-40% (5.0 V). Comparing the anodic potential of the LiTFSI-60% with/without LATP, both gave 4.7 V. These results indicated that the electrochemical windows of electrolyte membranes were affected by the content of the LiTFSI content, which was stable in the potential range of 2.5–4.7 V.

Figure 6 shows the Electrochemical Impedance Spectroscopy (EIS) results and the equivalent circuit for the electrolyte membranes with various LiTFSI contents based on Li-Li symmetric cells. In the Nyquist plots, the impedance spectra are comprised of one semicircle and one inclined line. The R_b is the electrolyte's resistance value and R_{inf} is the interface impedance between the electrolyte and the electrodes (containing charge transfer and electrode resistance). The interface impedance with the electrolyte, *CPE* is the electric double layer capacitor, *W* is the Warburg impedance of the diffusion reaction. The R_b, R_{inf}, and the total resistance (R_{total}) of the electrolyte membrane test results were determined by software using the equivalent circuit, and the ionic conductivity was calculated by using Equation (1) [37] and the results are listed in Table 2.

$$\sigma = L/(R_b \times S) \tag{1}$$

where, σ (S cm^{-1}) is the ionic conductivity, L (cm) is the thickness, S (cm^2) is the surface area of the electrolyte membrane and R_b (Ω) is the bulk resistance.
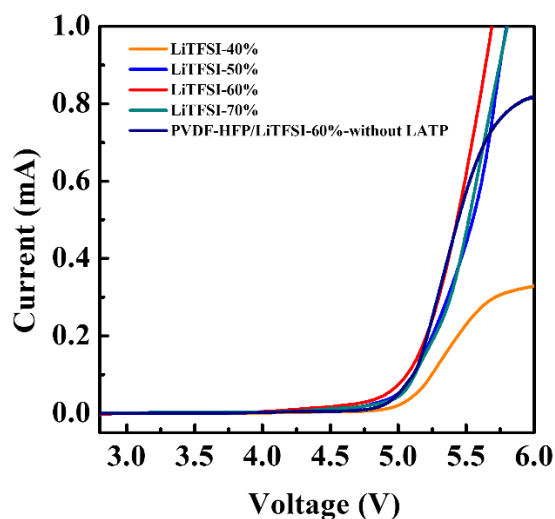

Figure 5. Linear sweep voltammetry curves of hybrid electrolyte with different contents of LiTFSI at room temperature with scan rate 10 mVs^{-1}.

The electrolyte resistance R_b and interface resistance (R_{inf}) apparently decreased from 342.2 Ω to 59.5 Ω and 805.3 Ω to 175.5 Ω, respectively, as the LiTFSI content increased from 40% to 60%. The LiTFSI-60% exhibited a maximum ionic conductivity of 2.14×10^{-4} S cm^{-1}, which was 1.86 times that of the LiTFSI-40%. This result indicated that the LiTFSI lithium salt improved the lithium-ion mobility in PVDH-HFP polymer due to the lower crystallinity of PVDH-HFP polymer and higher concentration of lithium-ions as the LiTFSI content increased. In addition, the interface resistance between the solid electrolyte membrane and lithium metal electrode decreased, due to a softer interfacial contact as the content of LiTFSI increased. As the content of LiTFSI increased to 70%, the R_b was 34.8 Ω, which was lower than that of the LiTFSI-60% (59.5 Ω). However, R_{inf} of the LiTFSI-70% was 285.3 Ω, which was apparently higher than that of the LiTFSI-60% (175.5 Ω), due the micro-crack of the LiTFSI-70% which was observed in the SEM micrograph (Figure 2d).
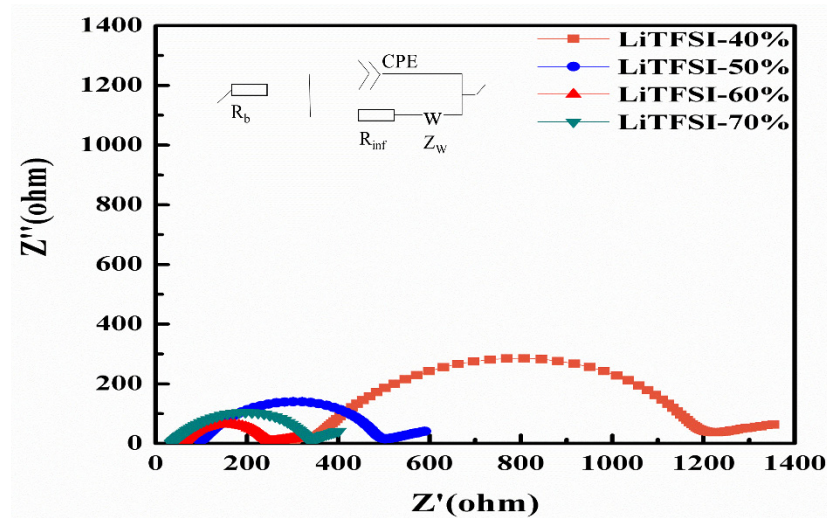

Figure 6. AC impedance spectra of electrolyte membranes made of different LiTFSI contents at 25 °C.

Table 2. The resistances and ionic conductivity of the Li/electrolytes/Li symmetry cells.

Sample	R_b (Ω)	R_{inf} (Ω)	R_{total} (Ω)	σ (S cm^{-1})
LiTFSI-40%	342.2	805.3	1147.5	6.85×10^{-5}
LiTFSI-50%	99.4	375.1	474.5	1.28×10^{-4}
LiTFSI-60%	59.5	175.5	235.1	2.14×10^{-4}
LiTFSI-70%	34.8	285.3	320.2	3.22×10^{-4}

The value of σ is calculated from the R_b.

Based on the results of mechanical properties, LSV and EIS of the solid electrolytes with various LiTFSI contents, it was concluded that the LiTFSI-60% was the optimal solid electrolyte membrane, which exhibited wide electrochemical windows of 2.5–4.7 V and high ionic conductivity of 2.14×10^{-4} S cm^{-1}. Figure 7 shows the charge–discharge performance of CR2032 ion cells, tested with LiFePO$_4$ cathode/LiTFSI-60% solid electrolyte/Li metal anode. Figure 7a displays the charge/ discharge curves of the cell at 0.1 C after 5 cycles. The discharge capacity of the cell was 98.8 mA h g^{-1} and remained at 97.3 mA h g^{-1} after the 5th cycle with 99% retention. Figure 7b shows charge–discharge curves of the cell at different C-rates. The discharge capacity of the cell decreased 14.4% from 99.66 to 85.28 mA h g^{-1} as the rate increased from 0.1 C to 0.2 C. The capacity of the cell quickly decreased to 41 mA h g^{-1} and 2 mA h g^{-1} as the rate increased to 0.5 C, then to 1 C. Therefore, this cell could be used in energy-type applications, but not for power-typed applications, due to its high polarization. Figure 7c shows the cycling performance of the cell. The cell showed a stable discharge capacity in the range of 95–104 mA h g^{-1} after 50 cycles with 95–100% coulombic efficiency. The cell based on LiTFSI-60% solid electrolyte showed an acceptable discharge capacity and stable cycle performance. However, the polarization was still too high compared to the cells based on traditional liquid electrolyte. This might have been due to the solid electrolyte being too thick, at about 80–100 μm [38]. The electrochemical performance of the cell is expected to improve when based on thin solid electrolyte in the future.
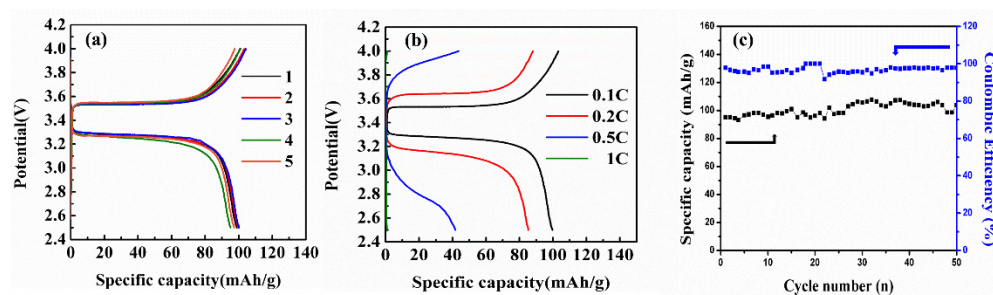

Figure 7. Charge and discharge curves of assembled solid state Li-ion battery with LiTFSI-60% hybrid electrolyte (**a**) different cycles at 0.1 C, (**b**) at different C-rates of 0.1 C, 0.2 C, 0.5 C and 1 C, and (**c**) cycle performance at 0.1 C.

3. Materials and Methods

Li$_{1.5}$Al$_{0.5}$Ti$_{1.5}$(PO$_4$)$_3$ (LATP) ceramic powder was synthesized by a citric acid-gel method [38]. Ti(OC$_4$H$_9$)$_4$ (Alfa, 98%), LiNO$_3$ (Alfa, 98%), Al(NO$_3$)$_3$.9H$_2$O (Alfa, 98%) and NH$_4$H$_2$(PO$_4$)$_3$ (J.T. Barker, 99%) were taken as the raw materials for the preparation of LATP. First, Ti(OC$_4$H$_9$)$_4$ was added to a 4:1 solution of deionized water and nitric acid followed by subsequent stirring. LiNO$_3$ and Al(NO$_3$)$_3$.9H$_2$O were added to the evenly mixed solution. Citric acid (Honeywell, 99%) was added at a molar ratio of 1.5 times of the total metal ion in the solution. Ammonia was added to the solution to adjust the pH to 5. NH$_4$H$_2$(PO$_4$)$_3$ and ethylene glycol were added under continuous stirring to dissolve in the solution. The required solution was heated for two hours at 120 °C, followed by heat treatment for three hours at 250 °C and calcined at 850 °C for 5 h to finally obtain crystalline powder of LATP.

Poly(vinylidene fluoride-hexafluoro propylene) (PVDF-HFP, Sigma, molecular weight: 400,000) and lithium bis(trifluoromethanesulfonyl)imide (LiTFSI, Alfa, purity: 98%) were dissolved in N-methyl pyrrolidone (NMP, Showa, purity: 95%) and heated and agitated on a magnetic stirrer at 40 °C for 24 h. Then LATP ceramic powder was added to the solution and mixed in a homogenizer for 0.5 h. The slurry was evenly deposited on the polymer substrate using a doctor blade, and then dried in a vacuum oven at 60 °C for 48 h to eliminate residual solvent. The dried electrolyte membranes were cut into 18 mm discs. The four samples based on various percentage of LITFSI lithium salt were labeled as LITFSI-40%, LITFSI-50%, LITFSI-60%, and LITFSI-70%.

A field-emission scanning electron microscope (FE-SEM, JSM 6701F, JEOL) was used to examine the morphology of the membranes. X-ray diffraction (XRD, D2 phaser, Bruker) was used to determine the crystalline phase of the LATP samples and hybrid electrolytes. Computer-based universal testing equipment (Ht-2402, Hung Ta) was used to measure the stress and strain curves for the hybrid electrolytes. The hybrid electrolytes' electrochemical windows were determined using linear sweep voltammetry (LSV) (Multichannel Electrochemical Workstation, Jiehan-5640) via the lithium foil (Li)/hybrid electrolyte/stainless steel (SS) sandwich cell at a scanning rate of 1 mV s^{-1}. Electrochemical impedance spectroscopy was used to measure ionic conductivities of hybrid electrolytes throughout a frequency range of 10^{-2} Hz to 10^6 Hz with 10 mV amplitude voltage (VSP-300, BioLogic, Grenoble, France). The charge–discharge of Li | 60% LiTFSI/PVDF-HFP/LATP | LiFePO$_4$ batteries were tested by the Battery Automation Test System (BAT-750B, Acu Tech, Taipei, Taiwan) in the range of 2.5–3.8 V at 0.1 C and 0.2 C.

4. Conclusions

In summary, a hybrid solid polymer/ceramics electrolyte, based on PVDF-HFP, LATP and LiTFSI, was fabricated and used in LiFePO$_4$/solid electrolyte/Li cells which exhibited good and stable electrochemical performance. The crystallization of PVDF-HFP-LATP decreased as the content of LiTFSI increased and this improved the lithium-ion mobility and contact between solid electrolyte and lithium metal electrode. The cell based on LiFePO$_4$ cathode/LiTFSI-60% solid electrolyte/Li metal anode showed a capacity of 98.8 mA h g^{-1} with stable discharge capacity in the range of 95–104 mA h g^{-1} with 95–100% coulombic efficiency after 50 cycles.

Author Contributions: D.M., Conceptualization, Methodology, Investigation, Data curation, Writing-original draft preparation; S.-Y.C., Investigation, Data curation, Formal analysis; I.-M.H., Conceptualization, Supervision, Funding acquisition, Writing-review and editing. All authors have read and agreed to the published version of the manuscript.

Data Availability Statement: The data that support the findings of this study are available from the corresponding author upon reasonable request.

Conflicts of Interest: The authors declare no conflict of interest.

References

1. Al Shaqsi, A.Z.; Sopian, K.; Al-Hinai, A. Review of energy storage services, applications, limitations, and benefits. *Energy Rep.* **2020**, *6*, 288–306. [CrossRef]
2. Divya, M.L.; Praneetha, S.; Lee, Y.-S.; Aravindan, V. Next-generation Li-ion capacitor with high energy and high power by limiting alloying-intercalation process using SnO$_2$@Graphite composite as battery type electrode. *Compos. Part B Eng.* **2022**, *230*, 109487–109493. [CrossRef]
3. Gür, T.M. Review of electrical energy storage technologies, materials and systems: Challenges and prospects for large-scale grid storage. *Energy Environ. Sci.* **2018**, *11*, 2696–2767. [CrossRef]
4. Zhu, C.; Han, K.; Geng, D.; Ye, H.; Meng, X. Achieving High-Performance Silicon Anodes of Lithium-Ion Batteries via Atomic and Molecular Layer Deposited Surface Coatings: An Overview. *Electrochim. Acta* **2017**, *251*, 710–728. [CrossRef]

5.   Divakaran, A.M.; Minakshi, M.; Bahri, P.A.; Paul, S.; Kumari, P.; Divakaran, A.M.; Manjunatha, K.N. Rational design on materials for developing next generation lithium-ion secondary battery. *Prog. Solid State Chem.* **2021**, *62*, 100298–100325. [CrossRef]

6.   Tsai, S.H.; Tsou, Y.L.; Yang, C.W.; Chen, T.Y.; Lee, C.Y. Applications of different nano-sized conductive materials in high energy density pouch type lithium ion batteries. *Electrochim. Acta* **2020**, *362*, 137166–137174. [CrossRef]

7.   Wang, W.; Li, Y.; Wang, Y.; Huang, W.; Lv, L.; Zhu, G.; Qu, Q.; Liang, Y.; Zheng, W.; Zheng, H. A novel covalently grafted binder through in-situ polymerization for high-performance Si-based lithium-ion batteries. *Electrochim. Acta* **2021**, *400*, 139442–139451. [CrossRef]

8.   Zhang, S.; Zhang, X. A novel non-experiment-based reconstruction method for the relationship between open-circuit-voltage and state-of-charge/state-of-energy of lithium-ion battery. *Electrochim. Acta* **2022**, *403*, 139637–139656. [CrossRef]

9.   Fang, H. Challenges with the Ultimate Energy Density with Li-ion Batteries. *IOP Conf. Ser. Earth Environ. Sci.* **2021**, *781*, 42023–42029. [CrossRef]

10. Eshetu, G.G.; Zhang, H.; Judez, X.; Adenusi, H.; Armand, M.; Passerini, S.; Figgemeier, E. Production of high-energy Li-ion batteries comprising silicon-containing anodes and insertion-type cathodes. *Nat. Commun.* **2021**, *12*, 5459–5473. [CrossRef]

11. Kwon, S.J.; Lee, S.E.; Lim, J.H.; Choi, J.; Kim, J. Performance and Life Degradation Characteristics Analysis of NCM LIB for BESS. *Electronics* **2018**, *7*, 406. [CrossRef]

12. Greim, P.; Solomon, A.A.; Breyer, C. Assessment of lithium criticality in the global energy transition and addressing policy gaps in transportation. *Nat. Commun.* **2020**, *11*, 4570–4581. [CrossRef] [PubMed]

13. Bobba, S.; Mathieux, F.; Blengini, G.A. How will second-use of batteries affect stocks and flows in the EU? A model for traction Li-ion batteries. *Resour. Conserv. Recycl.* **2019**, *145*, 279–291. [CrossRef] [PubMed]

14. Sanguesa, J.A.; Torres-Sanz, V.; Garrido, P.; Martinez, F.J.; Marquez-Barja, J.M. A Review on Electric Vehicles: Technologies and Challenges. *Smart Cities* **2021**, *4*, 372–404. [CrossRef]

15. Nitta, N.; Wu, F.; Lee, J.T.; Yushin, G. Li-ion battery materials: Present and future. *Mater. Today* **2015**, *18*, 252–264. [CrossRef]

16. Deng, D. Li-ion batteries: Basics, progress, and challenges. *Energy Sci. Eng.* **2015**, *3*, 385–418. [CrossRef]

17. Wang, M.S.; Wang, Z.Q.; Yang, Z.L.; Huang, Y.; Zheng, J.; Li, X. Carbon nanotube-graphene nanosheet conductive framework supported SnO_2 aerogel as a high performance anode for lithium ion battery. *Electrochim. Acta* **2017**, *240*, 7–15. [CrossRef]

18. Kong, L.; Yang, Y.; Li, R.; Li, Z. Phenylalanine-functionalized graphene quantum dot-silicon nanoparticle composite as an anode material for lithium ion batteries with largely enhanced electrochemical performance. *Electrochim. Acta* **2016**, *198*, 144–155. [CrossRef]

19. Thayumanasundaram, S.; Rangasamy, V.S.; Seo, J.W.; Locquet, J.P. Electrochemical performance of polymer electrolytes based on Poly(vinyl alcohol)/Poly(acrylic acid) blend and Pyrrolidinium ionic liquid for lithium rechargeable batteries. *Electrochim. Acta* **2017**, *240*, 371–378. [CrossRef]

20. Chen, Y.; Kang, Y.; Zhao, Y.; Wang, L.; Liu, J.; Li, Y.; Liang, Z.; He, X.; Li, X.; Tavajohi, N.; et al. A review of lithium-ion battery safety concerns: The issues, strategies, and testing standards. *J. Energy Chem.* **2021**, *59*, 83–99. [CrossRef]

21. Tong, Z.; Wang, S.B.; Liao, Y.K.; Hu, S.F.; Liu, R.S. Interface Between Solid-State Electrolytes and Li-Metal Anodes: Issues, Materials, and Processing Routes. *ACS Appl. Mater. Interfaces* **2020**, *12*, 47181–47196. [CrossRef] [PubMed]

22. Giraldo, S.; Nakagawa, K.; Vásquez, F.A.; Fujii, Y.; Wang, Y.; Miura, A.; Calderón, J.A.; Rosero-Navarro, N.C.; Tadanaga, K. Preparation of Composite Electrodes for All-Solid-State Batteries Based on Sulfide Electrolytes: An Electrochemical Point of View. *Batteries* **2021**, *7*, 77. [CrossRef]

23. Chen, X.; Guan, Z.; Chu, F.; Xue, Z.; Wu, F.; Yu, Y. Air-stable inorganic solid-state electrolytes for high energy density lithium batteries: Challenges, strategies, and prospects. *InfoMat* **2021**, *4*, e12248–e12268. [CrossRef]

24. Houache, M.S.E.; Yim, C.H.; Karkar, Z.; Abu-Lebdeh, Y. On the Current and Future Outlook of Battery Chemistries for Electric Vehicles-Mini Review. *Batteries* **2022**, *8*, 70. [CrossRef]

25. Verdier, N.; Foran, G.; Lepage, D.; Prébé, A.; Aymé-Perrot, D.; Dollé, M. Challenges in Solvent-Free Methods for Manufacturing Electrodes and Electrolytes for Lithium-Based Batteries. *Polymers* **2021**, *13*, 323. [CrossRef]

26. Liu, F.; Bin, F.; Xue, J.; Wang, L.; Yang, Y.; Huo, H.; Zhou, J.; Li, L. Polymer Electrolyte Membrane with High Ionic Conductivity and Enhanced Interfacial Stability for Lithium Metal Battery. *ACS Appl. Mater. Interfaces* **2020**, *12*, 22710–22720. [CrossRef]

27. Costa, C.M.; Lizundia, E.; Lanceros-Méndez, S. Polymers for advanced lithium-ion batteries: State of the art and future needs on polymers for the different battery components. *Prog. Energy Combust. Sci.* **2020**, *79*, 100846–100880. [CrossRef]

28. Ye, F.; Liao, K.; Ran, R.; Shao, Z. Recent Advances in Filler Engineering of Polymer Electrolytes for Solid-State Li-Ion Batteries: A Review. *Energy Fuels* **2020**, *34*, 9189–9207. [CrossRef]

29. Yao, Z.; Zhu, K.; Li, X.; Zhang, J.; Chen, J.; Wang, J.; Yan, K.; Liu, J. 3D poly(vinylidene fluoride–hexafluoropropylen) nanofiber-reinforced PEO-based composite polymer electrolyte for high-voltage lithium metal batteries. *Electrochim. Acta* **2022**, *404*, 139769. [CrossRef]

30. Feng, C.; Kyu, T. Role of dinitrile plasticizer chain lengths in electrochemical performance of highly conductive polymer electrolyte membrane for lithium ion battery. *Electrochim. Acta* **2020**, *330*, 135320–135331. [CrossRef]

31. Feng, J.; Wang, L.; Chen, Y.; Wang, P.; Zhang, H.; He, X. PEO based polymer-ceramic hybrid solid electrolytes: A review. *Nano Converg.* **2021**, *8*, 2–14. [CrossRef] [PubMed]

32. Liu, J.; Liu, T.; Pu, Y.; Guan, M.; Tang, Z.; Ding, F.; Xu, Z.; Li, Y. Facile synthesis of NASICON-type $Li_{1.3}Al_{0.3}Ti_{1.7}(PO_4)_3$ solid electrolyte and its application for enhanced cyclic performance in lithium ion batteries through the introduction of an artificial Li_3PO_4 SEI layer. *RSC Adv.* **2017**, *7*, 46545–46552. [CrossRef]

33. Yang, L.; Song, Y.; Liu, H.; Wang, Z.; Yang, K.; Zhao, Q.; Cui, Y.; Wen, J.; Luo, W.; Pan, F. Stable Interface between Lithium and Electrolyte Facilitated by a Nanocomposite Protective Layer. *Small Methods* **2020**, *4*, 1900751. [CrossRef]

34. Ling, S.G.; Peng, J.Y.; Yang, Q.; Qiu, J.L.; Lu, J.Z.; Li, H. Enhanced ionic conductivity in LAGP/LATP composite electrolyte. *Chin. Phys. B* **2018**, *27*, 038201–038208. [CrossRef]

35. Yang, H.; Bright, J.; Chen, B.; Zheng, P.; Gao, X.; Liu, B.; Kasani, S.; Zhang, X.; Wu, N. Chemical interaction and enhanced interfacial ion transport in a ceramic nanofiber-polymer composite electrolyte for all-solid-state lithium metal batteries. *J. Mater. Chem. A* **2020**, *8*, 7261–7272. [CrossRef]

36. Polu, A.R.; Rhee, H.W. Ionic liquid doped PEO-based solid polymer electrolytes for lithium-ion polymer batteries. *Int. J. Hydrogen Energy* **2017**, *42*, 7212–7219. [CrossRef]

37. Shi, X.; Ma, N.; Wu, Y.; Lu, Y.; Xiao, Q.; Li, Z.; Lei, G. Fabrication and electrochemical properties of LATP/PVDF composite electrolytes for rechargeable lithium-ion battery. *Solid State Ion.* **2018**, *325*, 112–119. [CrossRef]

38. Chen, S.Y.; Hsieh, C.T.; Zhang, R.S.; Mohanty, D.; Gandomi, Y.A.; Hung, I.M. Hybrid solid state electrolytes blending NASICON-type $Li_{1+x}Al_xTi_{2-x}(PO_4)_3$ with poly(vinylidene fluoride-co-hexafluoropropene) for lithium metal batteries. *Electrochim. Acta* **2022**, *427*, 140903–140912. [CrossRef]